Correlations Between XRD Peak Broadening and Elastic and Plastic Deformation for Mild Steel Sheets Under Tensile Loading

Sarra KHELIFI [1], Abdelhak AYAD [2, 3] *, Ahcène BOUMAIZA [1], Nadjet ROUAG [2], Francis WAGNER [4], Vincent JI [5]

[1] *Laboratoire de Physique de Rayonnement et Applications, Faculté des Sciences Exactes et Informatique, Université de Jijel, 18000 Jijel, Algeria*
[2] *Laboratoire Microstructures et Défauts dans les Matériaux, Faculté des Sciences Exactes, Univeristé Frères Mentouri Constantine 1, Route Ain El Bey, Constantine 25017, Algeria*
[3] *Département de Pharmacie, Faculté de Médecine, Université Salah Boubnider Constantine 3, Nouvelle ville Ali Mendjeli, Constantine 25005, Algeria*
[4] *LEM3 (UMR-CNRS 7239), Université de Lorraine -Metz, France*
[5] *ICMMO, Université Paris-Saclay, Bât-670, 91405 Orsay Cedex, France*

http://doi.org/10.5755/j02.ms.36098

Received 22 January 2024; accepted 2 April 2024

The polycrystalline nature of steel sheets plays a fundamental role in their plastic behavior during forming, especially under complex stresses, such as the deep drawing process. Heterogeneous microstructures cause variable internal stress levels, which strongly impact the material's macroscopic mechanical properties. X-ray diffraction (XRD) technique can be applied to determine microscopic internal stresses by peaks broadening analysis, which can be related to the degree of cold work at the microscopic level. As deep drawing is a complex deformation mode, an important motivating factor to perform such a study is to find the correlation between anisotropy and XRD peak broadening through tensile deformation tests. Therefore, the initial mechanical state and different deformed states were analysed by in-situ XRD peak broadening under tensile tests in various directions in the rolling plane of mild steel sheet, for both the elastic and plastic deformation domains. The results showed that the XRD peak broadening gives accurate estimations of deformation degrees. In the elastic domain, under realistic assumptions, a relation between the relative variation of peak broadening and the applied stress σ, like Hooke's law, was obtained by exploiting the linearity between the peak broadening and the elongation measured by the strain gauge. This formula may be used to deduce The Young's modulus. Interesting empirical relations between peak broadenings, macro deformations and hardness have been also established for the studied sheet in the plastic deformation region. Moreover, XRD peak broadenings were able to characterize the anisotropy of deformation in the rolling plane of the sheet. They are like the anisotropy coefficients in indicating the expected behavior under complex processes such as deep drawing by using ordinary tensile tests.
Keywords: XRD peak broadening, strain gauge, In-situ tensile loading, strain measurement, Young's modulus, anisotropy, mild steel.

1. INTRODUCTION

The interaction between neighboring grains must necessarily be considered in the study of the behavior of materials at the micro-scale which means at the scale of the grains. Indeed, the influence of local concentrations of deformations and stresses on the overall behavior of industrial materials intended for forming is crucial. The phenomena of localization which appear after complex deformations can lead to a strong decrease in ductility, and then to the fracture of the metallic material. The localization of deformation is a consequence of the presence of structural heterogeneities in the material (grain boundaries, precipitates, inclusions, and topological distribution of grains). The anisotropy of plastic properties is strongly involved in its behavior. In some cases, under the effect of complex stresses, the development of this anisotropy leads to harmful effects, but if it is well controlled, it can improve the plastic properties of sheets [1, 2].

In mild steel sheets, the presence of inclusions can play an important role in the localization of plastic deformation, and lead to development heterogeneity during deformation. Effectively, during loading, there is a concentration of stress around the inclusions, due to their higher Young's modulus compared to the matrix. The stronger stresses, which develop in the vicinity of inclusions, require localized plastic deformation. Deformation incompatibilities between the matrix and inclusions lead generally to their rupture or decohesion at the inclusion-matrix interface, depending on their relative strengths. It results, the formation of cavities within the matrix since the early stage of plastic deformation. This phenomenon may cause problems in the estimation of the superficial mechanical properties of materials intended for industrial applications [3 – 7].

Numerous research has been carried out to study accurately the local stresses and strains at the microscopic level by mechanical testing. There are several techniques for measuring strain in the tensile test, among these techniques:

* Corresponding author. Tel.: +213791023216; fax: +21331818870.
E-mail: *abdelhak.ayad@univ-constantine3.dz* (A. Ayad)

the strain gauge, optical strain measurement techniques, extensometer, strain measured by machine crosshead motion, geometric Moiré method, and others. Each technique has its advantages and inconveniences [8 – 11]. The accuracy and reliability of displacement measurements are often in question, as the magnitude of displacements is relatively small. X-ray diffraction peak broadening analysis of diffraction data from polycrystalline materials has shown its effectiveness in studying various microstructural properties. Indeed, when a metal is plastically deformed, the dislocation density increases, reducing the crystallites' size, i.e. the size of the coherent domain, and increasing the local strain in the crystallites. Both lead to broadening the diffraction peaks, which can be measured and used to quantify the deformation degree of material. This analysis allows obtaining information on the nature of dislocations and their densities using the modified Williamson Hall method for example, residual internal stresses and small lattice misfits around inclusions and precipitates [12 – 16]. Furthermore, the average magnitude of XRD peak broadening can be used as a means of quantifying the surface mechanical properties. It is related directly to the hardness, the elastic limit, or the degree of cold work of materials. Indeed, empirical relationships were found between the XRD peak width and the above-mentioned mechanical proprieties for Ni-Cr alloy under different simple deformation modes [17] and for carbon steel under tensile deformation, but only in the sheet's rolling direction [18].

Conventional strain gauges can also be adapted to determine the residual stresses and the degree of deformation for sheet steels and other materials and permit comparison between destructive and non-destructive measurements [19 – 22]. As an example, M.E. Turan et al. measured residual stress in steel rails using X-ray diffraction and strain gauge methods. They found that there is a direct proportional relationship and derived a formula between residual stress values obtained by the two methods based on the values of ten different rails [23].

As deep drawing is a complex deformation mode, an important motivating factor to perform such a study is to find the correlation between anisotropy and XRD peak broadening through simple deformation tests, i.e., tensile loadings. Therefore, the aim of this work is to study the influence of deformation on XRD peak broadening using several macroscopic deformation degrees obtained from in situ tensile tests in several directions in the plane of an aluminum-killed steel sheet. Thus, the degrees of plastic deformation are correlated to the widths of the diffraction peak either for the elastic and plastic deformation domains and compared to the values obtained by strain gauge. This comparison is very important for an accurate estimation of the internal deformations at the micro-scale. Empirical relationships between the macro deformation and hardness were also obtained from tensile tests in several rolling plane directions. Furthermore, the XRD peak broadening technique is used to characterize the anisotropy of deformation and some deep drawing issues in the studied steel sheet.

2. EXPERIMENTAL DETAILS

2.1. Specimens and experimental conditions

The investigated material is aluminum-killed steel (Al-K) of 1.5 mm thickness, obtained after a manufacturing thermo-mechanical cycle: hot rolling, cold rolling, and recrystallization annealing. The recrystallization annealing was carried out at 525 °C for 30 minutes, with a low heating rate. The chemical composition of this steel is shown in Table 1.

Table 1. The chemical composition of the studied steel

Element	C	Si	Mn	Cr	S	P	Ni	Al	N
wt.% × 10^{-3}	67	17	323	8	11	10	8	38	9

The in-situ tensile specimens were cut by laser with adequate geometry to the testing machine, with 5 mm width and a useful length of 20 mm (Fig. 1 a). The tensile tests were carried out using a universal testing machine connected by force capture.

In this study, two sample series were tested to compare the two strain measurement techniques: strain gauge and X-ray diffraction. Samples were first mechanically polished and then submitted to electrochemical polishing to eliminate the surface oxidation and the remaining micro polishing traces. Measurements were performed at the central region of the sample. The strain gauge was placed parallel to the specimen in the longitudinal direction. At each tensile step, the applied stresses and the corresponding deformations were measured. The longitudinal deformations were obtained by the gauge box and the loads by the force capture.

The sampling of the specimens at different α angles to the rolling direction is illustrated in Fig. 1 b.

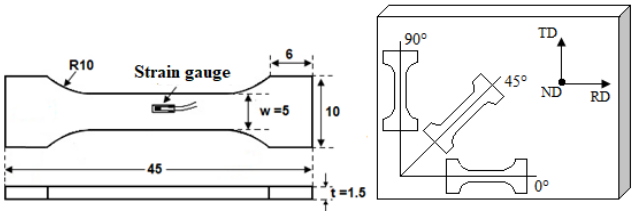

a b

Fig. 1. Specimen geometry and orientations for in-situ tensile tests: a – specimen geometry; b – specimens obtained at different α angles report to the rolling direction (RD) (all dimensions are in mm)

The third series is used to determine the macroscopic mechanical behavior at room temperature, such as yield strength ($R_{0.2\%}$), ultimate tensile strength (R_m), elongation ($A\%$), Lankford coefficient (r), planar anisotropy coefficient (Δr), and hardness. Vickers microhardness was ex-situ measured with a load of 200 g ($HV_{0,2}$) for the initial state and specimens with different deformation ratios (2, 3, 6, 9, 12, and 15 %) in the rolling direction (0°/RD). hardness values were obtained by averaging at least five measurement values for each sample.

Electron imagery and semiquantitative chemical analysis were performed using Zeiss Sigma 500 FEG-SEM

equipped with the Oxford Ultimax 65 Energy Dispersive X-ray Analysis (EDS).

2.2. Strain gauges

Strain gauge is one of the most popular methods used for strain measurement due to their evident accuracy, low cost, and simplicity. Nonetheless, they are frequently misused, and the reasons for measurement inaccuracy are underestimated [21 – 24]. The efficient operation of a strain gauge is entirely dependent on the contact and alignment with the testing sample. Due to bonding issues in the plastic section and at high strain rates, the strain gauge loses contact with tested pieces. Failure to make contact over even a small portion of the gauge will result in inaccurate strain indicators and findings cannot be considered as trustworthy. Only in the elastic section, the strain gauge can provide accurate values [12, 25 – 28].

In the elastic region, the apparent strain ε obtained from the force capture during the tensile test in a specimen with a rectangular cross-section area $S_0 = w_0 t_0$ is determined by Hooke's law:

$$\varepsilon = \frac{\sigma}{E} = \frac{(F/w_0 t_0)}{E}, \quad (1)$$

where σ is the applied stress; F is the corresponding acting force on the specimen's surface, E is the Young's modulus, W_0 and t_0 are the specimen width and thickness, respectively.

2.3. X-ray diffraction peak broadening

The used setup consists of an X-ray generator with a goniometric head, a linear detector (Elphyse), and a microprocessor (SET-X) that controls and analyses data. XRD investigation was performed on seven series of deformed samples using Cr-K$_\alpha$ radiation at 20 kV and 5 mA conditions to measure the broadened peak width.

XRD raw peaks have been recorded with Position Sensitive Detector (PSD) with an angular zone of 18° and a step of 0.04°. With a focusing optical system, the centering error of the incident beam and the diffraction beam is less than 0.1 mm compared to the goniometer rotation center; the sample position precision is more than 0.1 mm. The cumulated peak broadening error due to the XRD optical focus and mechanical systems is limited and not exceed 0.05°.

The {211} (2θ = 156.4°) family plane has been used to measure the peak broadening. For each measurement, 11 different ψ tilt angles, ranging from -37° to +37°, were averaged to provide good statistics on the peak width. For each ψ angle, the measurement time is 90 s. Measurements were obtained following an electrolytic polishing of the sample's surface, which removes at least 100 µm; the removed depth corresponds to the superficial cold working caused by sample fabrication. The irradiated area was a 2 mm diameter circle on the surface and 6 µm in depth, featuring 66 % absorption of the incident XRD beam.

SIEMENS S.A.'s DIFFRACT-AT software was used to analyze the peak broadening. Peaks have been fitted according to a Pseudo-Voigt function which gives the best fitting in our case [29]. Since we operate at fixed 2θ, the corresponding instrumental broadening for the studied {211} family plane is similar for each recording diffraction peak and has an inconsistent effect on peak broadening. Thus, the instrumental broadening was not subtracted from raw peaks.

The effect of diffraction Peak broadening was usually described as the peak broadening at some percentage of its height above the background. During surface enhancement, the peak width increases with the cold work degree. The approach used to assess the degree of cold work in deformed metals connects the X-ray diffraction peak broadening to the equivalent real plastic strain. If the degree of cold work is defined as the equal amount of actual plastic stress, the degree of cold work is cumulative and irrespective of the manner of deformation. The percent of cold work was assumed to represent the absolute value of the real plastic strain determined from changes in sample dimension. In this study, we mean by the peak width, the integral peak width (*IPB*), which is expressed as the diffraction peak surface area divided by its height, is used to describe the broadening evolution [18, 30 – 32].

3. RESULTS AND DISCUSSION

3.1. Regular mechanical properties of the sheet steel

The global industrial qualification of sheets before forming usually starts with the characterization of mechanical parameters. The initial value of the grain size is $d = (27 \pm 3)\ \mu m$, and the hardness $HV_{0,2} = 100 \pm 10$. In our case, tensile tests were carried out on a ZWICK universal testing machine using a constant crosshead speed of 0.2 cm/min. The average mechanical parameters were obtained (average value of 3 tests) by tensile tests up to fracture in rolling three directions toward the rolling direction (0°/RD, 45°/RD and 90°/RD). The corresponding macroscopic mechanical properties such as: elastic limit R_e, strength R_m, total elongation $A\%$ and the anisotropy coefficient r are listed in Table 2.

These tensile characteristics conform to the nominal values for the deep drawing mild steel process [33].

Table 2. Macroscopic mechanical properties of the sheet under study

Tensile directions	0°/RD	45°/RD	90°/RD
R_e, MPa	184,07	202.08	207.06
R_m, MPa	370.84	410.43	378.15
A, %	32.25	24.27	28.07
r	1.54	1.10	1.50

It should be noted that the coefficient of anisotropy presents a minimum for the 45°/RD direction. The mean value of Lankford coefficient r_m = 1.31, and the planar anisotropy coefficient Δr = 0.42. These coefficients of anisotropy are similar to the values reported by P.I. Welch and H.J. Bunge [34].

In general, good formability can only be obtained when the plastic deformation occurs homogeneously during the forming process and it satisfies the stability criteria, i.e., the Lankford coefficient $r > 1$ and the planar anisotropy coefficient Δr is close to zero. Otherwise, a poor surface

finish is obtained, and a premature failure may occur during the forming process.

3.2. Effect of inclusions and cavities on strain measurement

In many cases, the types of inclusions are more important than their amount [35, 36]. The presence of brittle inclusions including oxides in steel sheets, destroys the continuity of the steel matrix and leads to the stress concentration that would trigger cracks around them, thus reducing the performance of the steel sheet. Therefore, it is necessary to characterize and control the formation of the inclusions to improve the material behavior during the application industrial.

The most common problem of mild steel sheets intended for forming is cracking during parts manufacturing by deep drawing. Al-Killed steels contain mainly AlN precipitates. However, nonmetallic inclusions such as oxides (Al_2O_3) and sulfurs (MnS, Al_2S_3) can be embedded inside steel during the manufacturing process. Alumina inclusions on the surface of Al-killed steel attract each other to form clusters [37].

Effectively, Fig. 2 shows the SEM image and EDS analysis of the particles of the second phase observed on the surface of the sheet steel. The EDS spectrum analysis data indicates that most of the particles are most likely MnS inclusions (Fig. 2 a) and Al_2O_3 oxide clusters (Fig. 2 b). These populations react differently during the deformation. Thus, the distribution of stress will be heterogeneous in the clustered matrix [3, 35]. The existence of these different populations can lead to a rapid deformation localization at the grain scale and therefore to an early fracture.

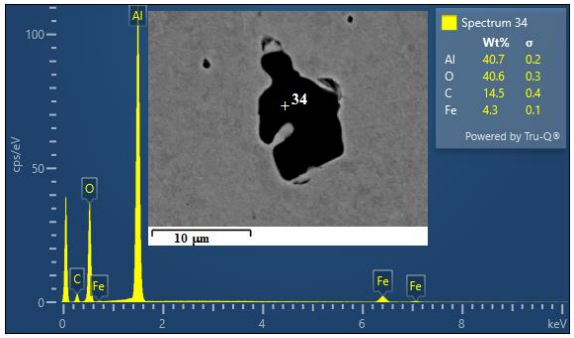

a

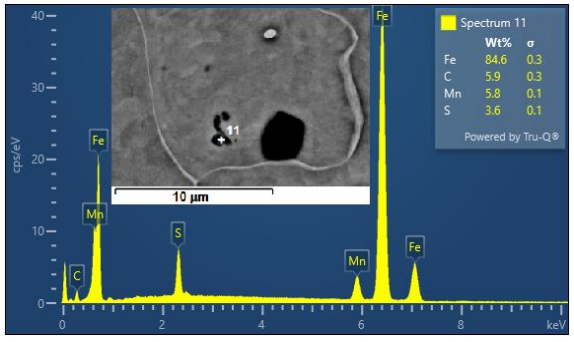

b

Fig. 2. EDS analysis of precipitates found in the studied steel, most likely are: a – Al_2O_3; b – MnS

Fig. 3 shows SEM-FEG micrographs taken from the surface of the specimen for the initial state and after deformation by deep drawing. It is clearly seen that the surface is characterized by the presence of inclusions and voids. Consequently, the existence of these various defects is also damaging for this type of steel since it gradually decreases the deformation capacity. This increases the likelihood of cracks or local thinning [38]. Fig. 3 b shows the appearance of damage to the interface matrix/inclusion and voids developed at the level of the matrix inclusion.

Generally, the most common sources of plastic strain in the materials intended for forming are dislocations, precipitates and inclusions, local chemical heterogeneities, existing stacking faults, twinning, long-range internal stresses, grain boundaries and sub-boundaries, internal stresses, local coherency strains or point defects. Dislocation generation and their movements are listed as the main sources of strain, since they are the major components in stacking faults and sub-boundaries and/or boundaries, and they can play an important role in the microscopic internal stresses and coherency strains [30].

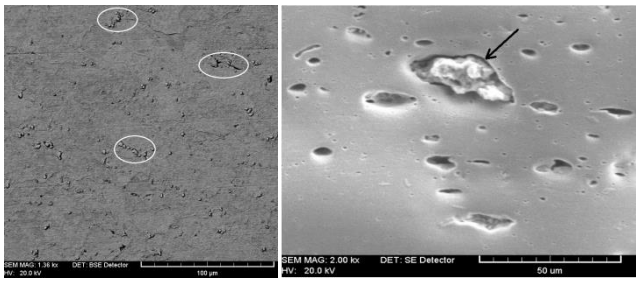

a b

Fig. 3. SEM images showing inclusions and voids on specimen's surfaces at two scales

3.3. Relationship between strain gauge and X-ray diffraction method for different applied loads in the elastic region

Fig. 4 shows the relationship between the X-ray peak broadening values and the elongations obtained by the strain gauge method in the elastic region for different applied loads from 0 to 160 MPa by in-situ tensile test.

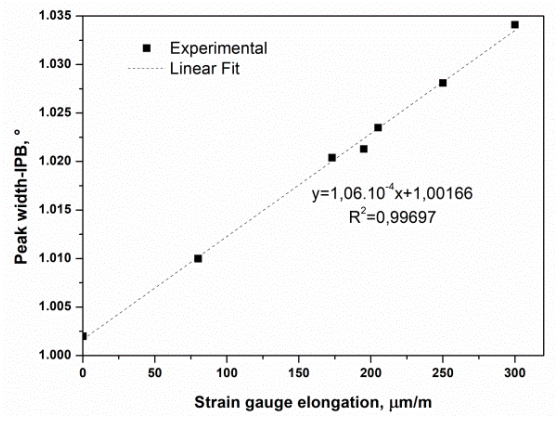

Fig. 4. Relationship between the {211} peak broadening and by the strain gauge elongations values for different applied load in the elastic region, i.e. from 0 to 160 MPa. The precision in IPB is less than 1 %

It should be noted the very good linear relationship between the two quantities, as follows:

$$IPB(°) = 106\,\varepsilon + 1.00166, \quad (2)$$

where the coefficient of determination (*R*-squared) is equal to 0.997.

The diffraction peak broadening (*IPB*) and strain gauge techniques give quasi-identical results in the elastic domain of the mild steel sheet. The values of the peak broadening and strain gauge correspond to reality.

The elastic microstrain measured by the strain gauge and the XRD peak broadening can be considered as equivalent to the macro-deformation that is given by Hooke's law (Eq. 1), if one considers the following assumptions:

1. the deformation is homogeneous at low strains and that deformation occurs only in the gauge region of the sample where the strain is defined as the elongation of the specimen relative to the original gauge length;
2. the number of the grains associated with the XRD peak broadening is statistically sufficient, leading to a micro strain, i.e. at the scale of the grains, that is representative of the specimen's global deformation. In our case, the X-ray analyzed area (3.14 mm^2) contains more than 4400 grains with a mean grain diameter of 30 μm, which is statistically significant.

By exploiting the linearity between the peak broadening and the elongation measured by the strain gauge in the domain of elastic deformation (Eq. 2), the relative variation of peak broadening can be expressed as:

$$\frac{\Delta(IPB)}{IPB_0} = \frac{IPB - IPB_0}{IPB_0} = 105.8\,\varepsilon, \quad (3)$$

where $IPB_0 = 1.00166$ is the initial value of the peak broadening.

A relation between the relative variation of peak broadening and the applied stress σ is then obtained by combining Eq. 1 and Eq. 3:

$$\frac{\Delta(IPB)}{IPB_0} = \frac{105{,}8}{E}\sigma. \quad (4)$$

This formula is similar to Hooke's law where the dependence between the relative variation of peak broadening and the stress is also linear. Furthermore the line slope of the plot $\frac{\Delta(IPB)}{IPB_0} = f(\sigma)$ is expressed as a function of the Young's modulus.

Young's Modulus is an experimentally derived value using strain and stress. Stress can be calculated, but strain must be measured which can be done using a strain gauge. However, if we consider the assumptions cited above, the peak broadening method can be used as an alternative method of strain gauge to calculate Young's modulus. The latter can be deduced from the line's slope of the graph $\frac{\Delta(IPB)}{IPB_0} = f(\sigma)$ which represents the value of $\frac{105.8}{E}$ for the steel under investigation.

It should be noted that, under the stated assumptions, this approach is correct and reproducible for the steel being studied. However, additional investigations are required to generalize it to other materials, which is outside the scope of the current study.

Estimations of strains, using the XRD peak broadening analysis and strain gauge measurements, are very interesting to show the quality and reliability of these techniques for the characterization of deformed materials in the elastic region. Furthermore, the XRD peak broadening analysis uncertainty is less than 0.05° and the corresponding precision of strain gauge measurements is around 2 %. Thus, the XRD peak broadening technique has been extended to study the plastic deformation domain at the expense of strain gauges.

3.4. Deformed surfaces morphology observation

The heterogeneous plastic deformation in the rolling plane is observed by FEG-SEM. The micro-graphical analysis showed that the micro-bands progress with an irregular form in this material during the deformation by tensile in different directions in the plane of the sheet. Fig. 5 a shows the morphology of the bands in the rolling direction obtained by an applied load of 300 MPa corresponding to the strain of 15 %. The surface morphology is composed of elongated deformation bands of two types (A and B). The deformation bands of type A develop predominantly during the early stage of deformation. They are bordered by interfaces that are oriented in the direction of maximum shear and have different mobilities. The geometry of the development of the micro-bands type B with the development of strains is illustrated in Fig. 5 b. This phenomenon may be correlated with the development of different slip systems. This heterogeneity behavior can lead locally to an important stress state that can provoke local thinning. Similar results have been published elsewhere [39, 40].

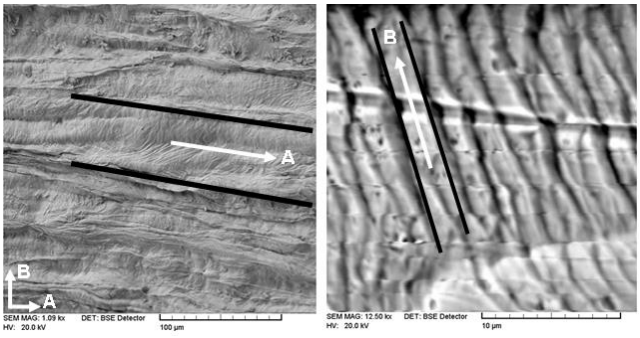

a b

Fig. 5. SEM-FEG micrographs of the deformed specimens at different scales showing the formation of reliefs and the morphology of micro-bands A and B

In general, the deformation microstructure is quite heterogeneous at high applied loads or stresses. It strongly depends on the orientation of grains and their slip plans in relationship with the macroscopic external loading direction. Therefore, measuring the local cumulative plastic average deformation by strain gauge is extremely challenging because of the heterogeneous strain distribution and evolution of the surface reliefs. In the range of 2 – 15 % total strain, errors were relatively larger (more than 2 % in relative). Due to this reason, the strain measurement using the strain gauge does not give the true values of the apparent deformation during the tensile testing. In this case, the use of the XRD peak broadening to determine the microscopic

internal strain is necessary. The method appears to be reliable for determining mechanical properties.

3.5. In-situ tensile tests and XRD peak broadening measurements of the specimens plastically deformed in the rolling plane

The variation of microhardness and peak broadening with deformation in the rolling direction (0°/RD) for the considered deformed states (2 – 15 % deformation degrees) are shown in Fig. 6. It is evident that the peak width is very sensitive to the metallurgical state of the studied steel, i.e. to the degree of cold work, and its corresponding hardness. The microhardness varies from 101 to 144 HV while the peak width increases from 1.002 to 1.414° for the considered deformed range. A linear variation is also observed between the peak width and hardness which can be expressed as follows:

$$\mathrm{HV} = 59.260 * IPB + 41.440 \quad (R^2 = 0{,}992). \tag{5}$$

A similar relationship between the {311} peak width and hardness was observed regardless of the deformation mode for an INCONEL 600 alloy [17].

Another empirical relation can be found between the peak broadening and the degree of deformation in this direction (0°/RD) as illustrated in Fig. 6 (see Eq. 6).

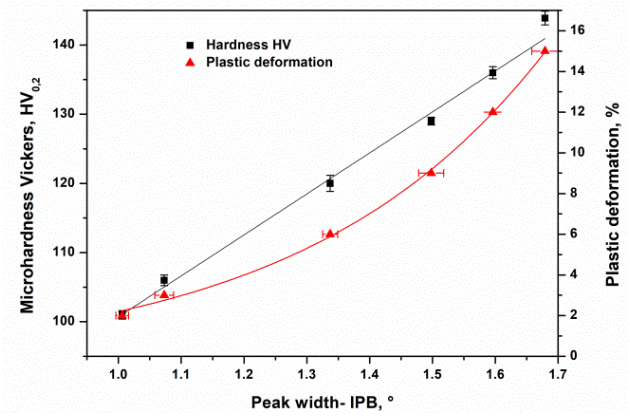

Fig. 6. Variation of the microhardness and the {211} peak broadening with tensile plastic deformation in the rolling direction (0°/RD) for the considered deformation rates (from 2 to 15 %)

Once the mechanical properties, the morphology of the surfaces and microstrains were characterized, the next steps are: first, to find empirical relations between diffraction peak broadening and plastic strain and then to use diffraction peak broadening to study the anisotropy of deformation in the sheet plane through three directions toward the rolling direction (0°/RD, 45°/RD and 90°/RD), and finally, to discuss the evolution of the peak broadenings during tensile in the selected deformation directions and their correlation to the anisotropy of deformation during deep drawing.

Fig. 7 presents the evolution of peak broadening during deformation in the above cited directions where three interesting semi-logarithmic empirical relationships between the diffraction peak broadenings and the plastic strain degree (ε_p) have been established (Eq. 6, Eq. 7, and Eq. 8).

$$(IPB)_{0^\circ} = 0.38348 * \ln(5.18188 * \varepsilon_p + 2.15675), \quad (R^2 = 0.99787); \tag{6}$$

$$(IPB)_{45^\circ} = 0.33103 * \ln(3.89529 * \varepsilon_p + 12.90655), \quad (R^2 = 0{,}99733); \tag{7}$$

$$(IPB)_{90^\circ} = 0.39663 * \ln(2.79587 * \varepsilon_p + 6.52526), \quad (R^2 = 0.99442). \tag{8}$$

As a result, equations that relate peak broadening to plastic strain are very useful since they allow macro strains to be estimated using peak broadening data, for just-finished pieces after forming or for the already used ones obtained from this steel. They can also be extrapolated to strain levels beyond those produced here.

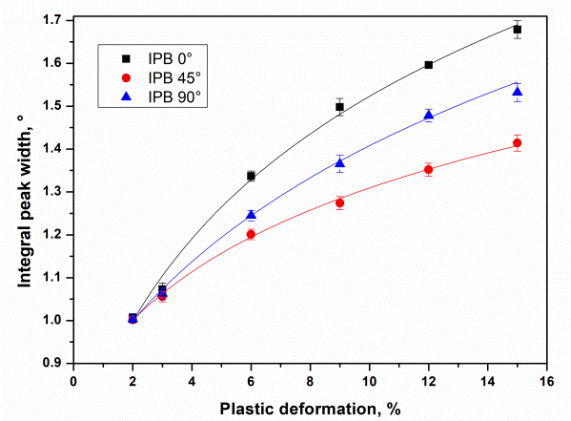

Fig. 7. Evolution of the {211} peak broadening with plastic tensile deformation in the three directions: 0°/RD, 45°/RD and 90°/RD of the steel sheet

In addition, when combining the overall data of plastic deformation's peak broadening, one can find the correlations between the peak broadening values for the different directions of deformation as presented in Eq. 9, Eq. 10, and Eq. 11. Examples of these correlations between $(IPB)_{90^\circ}$ and $(IPB)_{0^\circ}$ with $(IPB)_{45^\circ}$ are illustrated in Fig. 7.

$$(IPB)_{45^\circ} = 0.58576 * (IPB)_{0^\circ} + 0.41704, (R^2 = 0.99312); \tag{9}$$

$$(IPB)_{90^\circ} = 0.77998 * (IPB)_{0^\circ} + 0.21646, \ (R^2 = 0.99463); \tag{10}$$

$$(IPB)_{90^\circ} = 1.32853 * (IPB)_{45^\circ} + 0.33516, \ (R^2 = 0.99583). \tag{11}$$

It is evident that there are linear correlations between the various IPBs since the curve fittings produce linear dependencies with very good coefficients of determination. Using these equations, one can deduce the peak broadening in two directions with only the peak broadening values obtained from one direction. In addition, when combining them with Eq. 6, Eq. 7, and Eq. 8, the degree of deformation in these directions can be easily estimated. This allows us a considerable gain in time and material by avoiding cutting sheets in these directions to perform the tensile tests.

The X-ray diffraction peaks broadening is due either to the crystallite smallness (smaller than about a micrometer) or to the presence of dislocations in large enough abundance [17]. In our case, since plastic deformation is not severe, we expect less grain subdivision. The origin of the broadening

should then be mainly related to the strain field of dislocations. Hence, the impact of plastic deformation is evident during plastic deformation, the higher the plastic strain, the broader the peaks. The increase of plastic deformation leads to the formation of dislocation cell structures that implies an important micro-stress in these regions. Effectively, as illustrated in Fig. 7, the IPB increases with the deformation degree for the three tensile directions. However, deformations in the rolling direction (0°/RD) present the highest *IPB* values while the (45°/RD) direction possesses the lowest ones. If one takes 9% plastic strain as an example, the *IPB* values are 1.50, 1.27 and 1.36° for 0°/RD, 45°/RD and 90°/RD directions, respectively.

Indeed, if we consider $IPB = (IPB)_{45°}$ as a reference for peak broadening (Fig. 8), the peak broadenings $(IPB)_{0°}$ were found to be the highest ones, and $(IPB)_{0°}$ and $(IPB)_{90°}$ are both larger than $(IPB)_{45°}$. This trend increases progressively with increasing plastic deformation up to 15% elongation. At 15 % elongation the *IPB* values are $(IPB)_{0°} = 1.68°$, $(IPB)_{45°} = 1.41°$ and $(IPB)_{90°} = 1.53°$. It is interesting to note that the Lankford parameter (determined after 15 % elongation) varies in a similar way: $r(0°) = 1.54$, $r(45°) = 1.10$ and $r(90°) = 1.50$.

T. Ungar has considered, in a rather exhaustive way, the microstructural parameters that affect the X-ray diffraction peak broadening [30]. It is clear that in our case, the main effect is due to the increase of the dislocation density along plastic deformation, which produces a significant increase of the *IPB* in all three cases (Fig. 7). Moreover, the arrangement of the dislocations (trend to build walls or cells) that can differ because of the anisotropy also plays a role on the *IPB* [30] and, likely, explains the observed differences between the three cases 0°, 45° and 90°.

As mentioned above, the XRD peak broadenings are like the anisotropy coefficients; they can indicate the expected behavior during deep drawing where sheets are not subjected to a single mode of solicitation. The effect of plastic deformation anisotropy is apparent in the deep-drawing process where the crack initiation and propagation zone during manufacturing occur at a certain angle α relative to the rolling direction, depending on the applied stresses and the coefficient of anisotropy of the sheet. For example, Bao et al. [41] found that micro-cracks appear around 55° – 60°/RD direction for a steel sheet under unidirectional loadings. Indeed, the peak broadenings $(IPB)_{0°}$ and $(IPB)_{90°}$ were found to be greater than $(IPB)_{45°}$, indicating that this sheet experiences easier plastic deformation near 0°/RD and 90°/RD directions than near 45°/RD directions. The existence of these different behaviors may occur in regions with alternating high and low dislocation densities around the 45°/RD direction during deep drawing. Therefore, the anisotropy of deformation in the rolling plane may lead to local thinning or micro-cracking at the vicinity of this direction halting the homogeneous global deformation earlier than expected.

In addition to its good accuracy (more than 0.05° in 2θ), DRX peak broadening analysis is also considered a reliable method for the determination of superficial mechanical properties of materials in several industrial fields [42]. This method is very advantageous for mechanical behavior characterization especially when compared to other methods like the strain gauge which poses practical difficulties for plastic deformation measurement for steel sheets with marked structural anisotropy. It can be used to estimate the degree of plastic deformation and to indicate the anisotropy of deformation, to prevent rupture and any deep drawing issues.

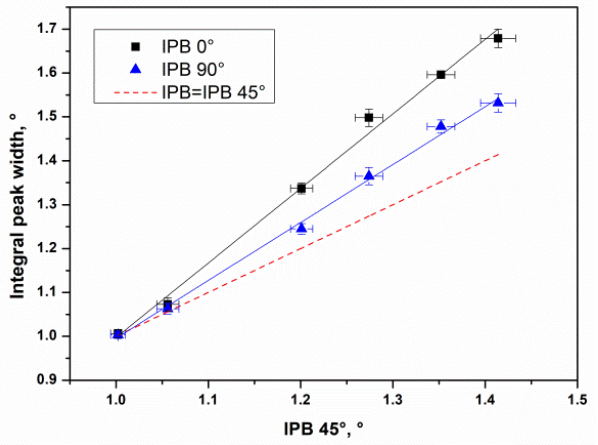

Fig. 8. Correlations between the peak broadenings $(IPB)_{0°}$ and $(IPB)_{90°}$ with $(IPB)_{45°}$ where the curves $IPB=f(IPB_{45°})$ have been plotted for $(IPB)_{0°}$ and $(IPB)_{90°}$

4. CONCLUSIONS

To obtain a better understanding of the mechanical behavior of mild steel sheets, characterization of their microstructure and mechanical properties at the scale of grains was performed.

The EDS examination revealed the presence of MnS inclusions and Al_2O_3 clusters in the steel matrix. Increasing the amount of deformation may induce stress concentration around them, resulting in micro-cracks and reducing the performance of the steel sheet.

Two strain measuring approaches are compared quantitatively by determining the internal strain (elastic and plastic strains) at the grain scale of the sheet. A comparative investigation was conducted to connect macrostrain with microstrain utilising a strain gauge and XRD peak broadening during in-situ deformation of samples acquired in the sheet's rolling plane.

It has been found that the peak broadening and strain gauge provided reliable data in the elastic region; the estimation of the measurement uncertainty for the parameters of the elastic region is very satisfactory. In addition, a linear relation similar to Hooke's law between the relative variation of the peak broadening and the applied stress has been established, it may allow us to deduce the Young's modulus value, at least for the studied steel.

In the plastic region, measurement of the strain by the strain gauge technique seems to be not very reliable. However, the peak broadening offers several advantages where empirical relationships have been developed relating the peaks broadening to the hardness and plastic strain's degree in the rolling plane. These relations may be used to correlate peak broadening data to the metallurgical state, for just-fabricated pieces after forming or for the already used ones obtained from this steel. The XRD peak broadening technique not only make it possible to evaluate certain mechanical parameters of the studied steel but also plays a role as the coefficients of anisotropy, in indicating the

anisotropy of deformation in the sheet's plane, to prevent rupture and any deep drawing issues such as local thinning or micro-cracking.

Acknowledgments

We would like to thank Prof. Silvia Barella and Mr. Rasheed Michael Ishola (Department of Mechanical Engineering, Politecnico di Milano, Italy) for SEM and EDS analysis. The authors S. K., A. A. and A. B. acknowledge financial support from the DGRSDT (MESRS-Algeria).

REFERENCES

1. **Hoc, T., Rey, C., Viaris de lesegno, P.** Mesostructure of the Localization in Prestrained Mild Steel *Scripta Materialia* 42 (8) 2000: pp. 749 – 754. https://doi.org/10.1016/S1359-6462(99)00425-X
2. **Delaire, F., Raphanel, J.L., Rey, C.** Plastic Heterogeneities of a Copper Milicrystal Deformed in Uniaxial Tension: Experimental Study and Finite Element Simulations *Acta Materialia* 48 (5) 2000: pp. 1075 – 1087. https://doi.org/10.1016/S1359-6454(99)00408-5
3. **Toribio, J., Ayaso, F.J., Rodríguez, R.** Evolution of Non-Metallic Inclusions With Cold Drawing in Progressively Cold Drawn Eutectoid Pearlitic Steel Wires *Procedia Structural Integrity* 33 2021: pp. 1209 – 1214. https://doi.org/10.1016/j.prostr.2021.10.137
4. **Qiu, G., Zhan, D., Li, C., Yang, Y., Qi, M., Jiang, Z., Zhang, H.** Influence of Inclusions on the Mechanical Properties of RAFM Steels Via Y and Ti Addition *Metals* 9 (8) 2019: pp. 851. https://doi.org/10.3390/met9080851
5. **Ånmark, N., Karasev, A., Jönsson, G.P.** The Effect of Different Non-Metallic Inclusions on the Machinability of Steels *Materials* 8 (2) 2015: pp. 751 – 783. https://doi.org/10.3390/ma8020751
6. **Yan, W., Chen, W., Li, J.** Quality Control of High Carbon Steel for Steel Wires *Materials* 12 2019: pp. 846. https://doi.org/10.3390/ma12060846
7. **Li, H.B., Huang, Q.X., Zhou, C.L., Liu, G.M., Ma, Q.** Stainless Steel Microstructural Evolution of Hot-Rolled Clad Plate *Materials Science (Medžiagotyra)* 22 (4) 2016: pp. 495 – 500. https://doi.org/10.5755/j01.ms.22.4.12828
8. **Adamczak, S., Bochnia, J., Kundera, C.** Stress and Strain Measurements in Static Tensile Tests *Metrology and Measurement Systems* XIX (3) 2012: pp. 531 – 540. https://doi.org/10.2478/v10178-012-0046-3
9. **Pesci, R., Inal, K., Masson, R.** Stress Distribution and Cleavage Analysis in a 16MnNiMo5 Bainitic Steel X-ray Diffraction and Multiscale Polycrystalline Modeling *Journal of Materials Science and Technology* 20 2004: pp. 32 – 34. https://www.jmst.org/EN/Y2004/V20/ISupl./32
10. **Xia, L.W., Xia, Y.M., Xia, C.G., Liang, Y., Chao, L., Guo, Y., Liu, K.** An Experimental Study on the Tensile Mechanical Behavior of Steel Cords for Radial Tires *Journal of Experimental Mechanics* 17 (3) 2002: pp. 307 – 314. http://doi.org/10.3969/j.issn.1001-4888.2002.03.011
11. **Lord, J.D., Morrell, R.** Elastic Modulus Measurement-Obtaining Reliable Data from the Tensile Test *Metrologia* 47 (2) 2010: pp. S41 – S49. http://doi.org/10.1088/0026-1394/47/2/S05
12. **Montero, W., Farag, R., Díaz, V., Ramirez, M., Boada, B.L.** Uncertainties Associated with Strain-Measuring Systems Using Resistance Strain Gauges *Journal of Strain Analysis for Engineering Design* 46 (1) 2011: pp. 1 – 13. http://sdj.sagepub.com/content/46/1/1
13. **Willink, R.** On the Uncertainty of the Mean of Digitized Measurements *Metrologia* 44 2007: pp. 73 – 81. http://iopscience.iop.org/0026-1394/44/1/011
14. **Pinheiro, B., Lesage, J., Pasqualino, I., Benseddiq, N., Bemporad, E.** X-ray Diffraction Study of Microstructural Changes During Fatigue Damage Initiation in Steel Pipes *Materials Science and Engineering A* 532 2012: pp. 158 – 166. https://doi.org/10.1016/j.msea.2011.10.07
15. **Wang, X.L., Wang, Y.D., Stoica, A.D., Horton, D.J., Tian, H., Liaw, P.K., Choo, H., Richardson, J.W., Maxey, E.** Inter- and Intragranular Stresses in Cyclically-deformed 316 Stainless Steel *Materials Science and Engineering A* 399 2005: pp. 114 – 119. https://doi.org/10.1016/j.msea.2005.02.030
16. **Liu, H., Wei, X., Xing, S., Wang, L., Zhu, W., Jiang, C., Ji, V., Zhan, K.** Effect of Stress Shot Peening on the Residual Stress Field and Microstructure of Nanostructured Mg-8Gd-3Y Alloy *Journal of Materials Research and Technology* 10 2021: pp. 74 – 83. https://doi.org/10.1016/j.jmrt.2020.11.085
17. **Ji, V., Zhang, Y.G., Chen, C.Q.** The Non-Destructive Estimation of the Superficial Mechanical Properties of Components in the INCONEL 600 Alloy by X-ray Diffraction Peak Width *Surface and Coatings Technology* 130 2000: pp. 95 – 99. https://doi.org/10.1016/S0257-8972(00)00683-6
18. **Boumaiza, A., Ji, V., Rouag, N.** The Nondestructive Estimation of Mechanical Properties of a Carbon Steel by X-Ray Diffraction Peak Broadening *Journal of Testing and Evaluation* 37 (4) 2009: pp. 343 – 346. http://doi.org/10.1520/jte102083
19. **Joo, H.D., Kim, J.S., Kim, K.H., Tamura, N., Koo, Y.M.** In Situ Synchrotron X-ray Microdiffraction Study of Deformation Behavior in Polycrystalline Coppers during Uniaxial Deformations *Scripta Materialia* 51 2004: pp. 1183 – 1186. https://doi.org/10.1016/j.scriptamat.2004.07.003
20. **Ebner, S., Schnitzer, R., Maawad, E., Suppan, C., Hofer, C.** Influence of Partitioning Parameters on the Mechanical Stability of Austenite in a Q&P steel: A Comparative In-situ Study *Materialia* 15 2021. pp: 101033 – 101042. https://doi.org/10.1016/j.mtla.2021.101033
21. **Window, A.L., Holister, G.S.** Strain Gauge Technology, 2nd ed., Applied Science Publishers, London 1992. https://doi.org/10.1017/S0001924000019291
22. **Goanta, V.** Extensometer for Determining Strains on a Tensile and Torsion Simultaneous *Sensors* 20 (2) 2020: pp. 385. https://doi.org/10.3390/s20020385
23. **Turan, M.E., Aydin, F., Sun, Y., Çetin, M.** Residual Stress Measurement by Strain Gauge and X-ray Diffraction Method in Different Shaped Rails *Engineering Failure Analysis* 96 2019: pp. 525 – 529. https://doi.org/10.1016/j.engfailanal.2018.10.016
24. **Mutoh, Y., Korda, A.A., Miyashita, Y., Sadasue, T.** Stress Shielding and Fatigue Crack Growth Resistance in Ferritic-Pearlitic Steel *Materials Science and Engineering A* 468 – 470 2007: pp. 114 – 119.

https://doi.org/10.1016/j.msea.2006.07.171

25. **Motra, H.B., Hildebrand, J., Dimmig-Osburg, A.** Assessment of Strain Measurement Techniques to Characterise Mechanical Properties of Structural Steel *Engineering Science and Technology, an International Journal* 17 2014: pp. 260 – 269. http://dx.doi.org/10.1016/j.jestch.2014.07.006
26. **Serban, A., Barsanescu, P.D.** Automatic Detection of the Orientation of Strain Gauges Bonded on Composite Materials with Polymer Matrix in Order to Reduce the Measurement Errors *Polymers* 15 (4) 2023: pp. 876. https://doi.org/10.3390/polym15040876
27. **Chandra, P.V.C.S., Manoj, A., Swathi, B.R.** Residual Stress Measurement of Inconel 600 on Different Welding Techniques by Using Conventional and XRD Methods *Materials Today: Proceedings* 41 (5) 2021: pp. 1160 – 1163. https://doi.org/10.1016/j.matpr.2020.09.403
28. **Magalhães, R.R., Junior, A.B.V., Barra, S.R.** The Use of Conventional Strain Gauges Evaluation for Measurements of Residual Stresses in Welded Joints *Journal of the Brazilian Society of Mechanical Sciences and Engineering* 36 2014: pp. 173 – 180. https://doi.org/10.1007/s40430-013-0082-2
29. **Wertheim, G.K., Butler, M.A., West, K.W., Buchanan, D.N.E.** Determination of the Gaussian and Lorentzian Content of Experimental Line Shapes *Review of Scientific Instruments* 45 1974: pp. 1369 – 1371. https://doi.org/10.1063/1.1686503
30. **Ungar, T.** Microstructural Parameters from X-ray Diffraction Peak Broadening *Scripta Materialia* 51 2004: pp. 777 – 778. https://doi.org/10.1016/j.scriptamat.2004.05.007
31. **Arne, E., Berthold, S.** The Strength Differential Effect in Different Heat Treatment Conditions of the Steels 42CrMoS4 and 100Cr6 *Materials Science & Engineering A* 620 2015: pp. 262 – 272. http://dx.doi.org/10.1016/j.msea.2014.10.027
32. **Sarkar, A., Mukherjee, P., Barat, P.** X-ray Diffraction Studies on Asymmetrically Broadened Peaks of Heavily Deformed Zirconium-Based Alloys *Materials Science and Engineering A* 485 2008: pp. 176 – 181. https://doi.org/10.1016/j.msea.2007.07.063
33. **Bouras, M., Boumaiza, A., Ji, V., Rouag, N.** XRD Peak Broadening Characterization of Deformed Microstructures and Heterogeneous Behavior of Carbon Steel *Theoretical and Applied Fracture Mechanics* 61 2012: pp. 51 – 56. http://dx.doi.org/10.1016/j.tafmec.2012.08.006
34. **Welch, P.I., Bunge, H.J.** Influence on Grain Size on Plastic Anisotropy in Low-carbon Steels *Materials Science and Technology* 2 1986: p. 354. https://doi.org/10.1179/mst.1986.2.4.354
35. **Guo, X., Tan, M., Li, T., Ju, L., Dang, J., Guo, H., Zhao, Y.** Formation Mechanisms and Three-Dimensional Characterization Of Composite Inclusion of MnS-Al_2O_3 in High Speed Wheel Steel *Materials Characterization* 197 2023: p. 112669. https://doi.org/10.1016/j.matchar.2023.112669
36. **Choudhary, P., Garrison, W.M.** The Effect of Inclusion Type on the Toughness of 4340 Steel *Materials and Manufacturing Processes* 25 2010: pp. 180 – 184. https://doi.org/10.1080/10426910903221138
37. **Kimura, S., Nakajima, K., Mizoguchi, S.** Behavior of Alumina-Magnesia Complex Inclusions and Magnesia Inclusions on the Surface of Molten Low-Carbon Steels *Metallurgical and Materials Transactions B* 32 2001: pp. 79 – 85. https://doi.org/10.1007/s11663-001-0010-1
38. **Boumaiza, A., Rouag, N., Baudin, T., Penelle, R.** SEM-EBSD Observations of Crack Initiation and Propagation Due to Orientation Changes During Forming in Mild Steel *Advanced Materials Research* 682 2013: pp. 25 – 32. https://doi.org/10.4028/www.scientific.net/AMR.682.25
39. **Han, J.H., Kim, D.I., Jee, K.K., Oh, K.H.** In-situ Orientation Rotation Behavior Study During Tensile Deformation of Aluminum Single Crystal and Polycrystal *Materials Science Forum* 449 – 452 2004: pp. 593 – 596. https://doi.org/10.4028/www.scientific.net/MSF.449-452.593
40. **Kim, K.H., Koo, Y.M.** In-situ X-ray Diffraction Study About Uniaxial Deformation Behavior in a Copper Single Crystal *Materials Science and Engineering* 335 2002: pp. 309 – 312. https://doi.org/10.1016/S0921-5093(01)01943-8
41. **Bao, C., Francois, M., Le Joncour, L.** A Closer Look at the Diffuse and Localised Necking of a Metallic Thin Sheet: Evolution of the Two Bands Pattern *Strain* 52 2016: pp. 244 – 260. https://doi.org/10.1111/str.12184
42. **Chai, Z., Huang, X., Xu, J., Yu, Z., Ji, V., Jiang, C., Chen, X.** Kinetics and energetics of room-temperature microstructure in nanocrystalline Cu films: The grain-size dependent intragrain strain energy *Journal of Applied Physics* 131 2022: pp. 055301. https://doi.org/10.1063/5.0068020